CORRECTED 22 APRIL 2025; SEE LAST PAGE

SCIENCE ADVANCES | RESEARCH ARTICLE

CELL BIOLOGY

Morphogenesis of bacterial cables in polymeric environments

Sebastian Gonzalez La Corte[1], Corey A. Stevens[2], Gerardo Cárcamo-Oyarce[2,3], Katharina Ribbeck[2], Ned S. Wingreen[4]*, Sujit S. Datta[5,6]*

Many bacteria live in polymeric fluids, such as mucus, environmental polysaccharides, and extracellular polymers in biofilms. However, laboratory studies typically focus on cells in polymer-free fluids. Here, we show that interactions with polymers shape a fundamental feature of bacterial life—how they proliferate in space in multicellular colonies. Using experiments, we find that when polymer is sufficiently concentrated, cells generically and reversibly form large serpentine "cables" as they proliferate. By combining experiments with biophysical theory and simulations, we demonstrate that this distinctive form of colony morphogenesis arises from an interplay between polymer-induced entropic attraction between neighboring cells and their hindered ability to diffusely separate from each other in a viscous polymer solution. Our work thus reveals a pivotal role of polymers in sculpting proliferating bacterial colonies, with implications for how they interact with hosts and with the natural environment, and uncovers quantitative principles governing colony morphogenesis in such complex environments.

INTRODUCTION

Many bacteria live in polymeric fluids, such as mucus that lines the airways, gut, and cervico-vaginal tract in the body (*1*, *2*), exopolymers in the ocean (*3*), and cell-secreted extracellular polymeric substances (EPSs) that encapsulate biofilms (*4*). However, laboratory studies of bacteria typically focus on cells in polymer-free fluids. As a result, despite their prevalence, how extracellular polymers influence bacterial behavior remains poorly understood.

Recent work hints that interactions with polymers can dramatically alter how individual motile cells swim (*5*–*8*) and aggregate with other cells (*9*–*13*). Nevertheless, the possible influence of polymers on another fundamental characteristic of bacterial life—spatial proliferation in a multicellular colony (*14*, *15*)—remains unknown. Colony morphology can be biologically important. For example, studies of bacteria proliferating on planar surfaces show that their resulting colonies can exhibit a variety of morphologies (*14*, *16*–*25*), which in turn can affect cell-cell signaling (*26*), genetic diversity (*27*–*30*), and colony resilience and susceptibility to external stressors (*9*, *31*, *32*). Hence, we ask: Do interactions with polymers sculpt the morphology of proliferating bacterial colonies?

Here, we demonstrate that this is indeed the case, and we elucidate the underlying mechanisms. In nature, many bacteria are nonmotile or lose motility (*33*–*56*), but still continue to proliferate in colonies; indeed, the loss of flagella is often associated with pathogenesis and bacterial adaptation to diseased mucosal environments, such as in cystic fibrosis. Therefore, we focus on the spatial proliferation of rod-shaped, nonmotile mutant cells that lack flagella. By performing experiments with these bacteria in polymer solutions, we find that when polymer is sufficiently concentrated, cells form large-scale "cables" as they proliferate in a colony—in stark contrast to forming a random dispersion, as in the conventionally studied polymer-free case. This characteristic cable morphology arises independent of variations in cell type and polymer composition across three different species of bacteria and seven different polymers, including mucins, a key component of mucus in the body. By combining experiments, theoretical modeling, and agent-based simulations, we trace the origin of cable formation to an interplay between polymer-induced entropic attraction between neighboring cells and their hindered ability to diffusively separate from each other after growth and division in a viscous polymer solution. Our work thus reveals a pivotal role of polymers in shaping proliferating bacterial colonies and provides quantitative principles to predict and control these morphodynamics more broadly.

RESULTS

Nonmotile bacteria proliferating in polymer solutions form long multicellular cables across different species and solution compositions

We use confocal microscopy to directly visualize nonmotile bacteria, constitutively expressing green fluorescent protein (GFP) in their cytoplasms, as they proliferate in nutrient-rich solutions with polymers added at a defined mass concentration c. To start, we use *Escherichia coli* as a model bacterium and mucus obtained from human primary transverse colon cells (*57*) as the polymer solution. In polymer-free solution, the cells continually grow, divide, separate from each other, and thermally diffuse apart, eventually forming a random dispersion (Fig. 1A and movie S1). Colony morphogenesis is completely different in the mucus solution: Cells pack side-by-side up to a limited bundle size and then remain oriented end-to-end for subsequent divisions, eventually forming an intertwined network of long, serpentine, multicellular cables (Fig. 1B and movie S2). This phenomenon is not dependent on the source of the mucus: We observe similar colony morphologies using purified native porcine intestinal mucin (Muc2) at $c = 0.5\,\%\,\mathrm{w/v}$ (fig. S6 and movie S3), which is also representative of human intestinal mucus (*1*, *2*).

[1]Lewis-Sigler Institute for Integrative Genomics, Princeton University, Princeton, NJ, USA. [2]Department of Biological Engineering, Massachusetts Institute of Technology, Cambridge, MA, USA. [3]Facultad de Ciencias Biológicas, Facultad de Medicina, Pontificia Universidad Católica de Chile, Santiago, Chile. [4]Department of Molecular Biology, Princeton University, Princeton, NJ, USA. [5]Division of Chemistry and Chemical Engineering, California Institute of Technology, Pasadena, CA, USA. [6]Department of Chemical and Biological Engineering, Princeton University, Princeton, NJ, USA.
*Corresponding author. Email: wingreen@princeton.edu (N.S.W.); ssdatta@caltech.edu (S.S.D.)

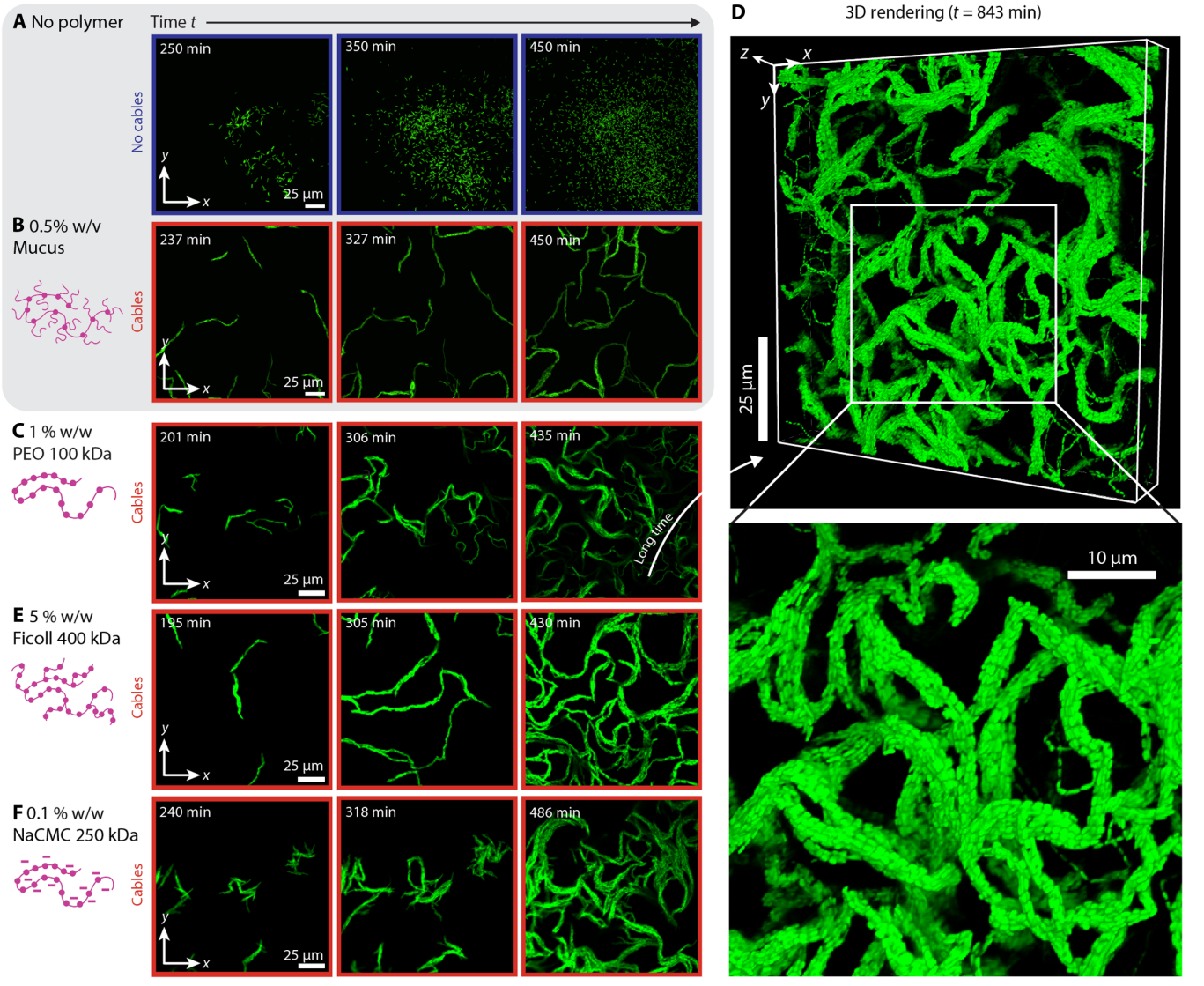

Fig. 1. Nonmotile *E. coli* generically form cables as they proliferate in polymer solutions. (**A**) Time sequence of nonmotile *E. coli* proliferating in nutrient-rich polymer-free fluid; the cells form a random dispersion. (**B**, **C**, **E**, and **F**) Same as in (A), but with added (B) mucus (0.5% w/v), (C) PEO 100 kDa (1% w/w), (E) Ficoll 400 kDa (5% w/w), or (F) NaCMC 250 kDa (0.1% w/w); in these polymeric fluids, cells form large, serpentine cables. Full dynamics can be seen in movies S1 to S6. (**D**) Three-dimensional rendering of a small volume of the colony shown in (C) after 843 min from the initiation of imaging, showing the internal structure of cables.

To explore the generality of cable formation, we repeat this experiment, but replacing the mucins—which are known to adsorb to bacterial cells (*58*–*62*)—with 100-kDa polyethylene oxide (PEO), a chemically inert, uncharged, nonadsorbing, synthetic polymer (*63*–*66*). For sufficiently concentrated PEO solutions, we again observe cable formation, as exemplified by the confocal micrographs in Fig. 1C and movie S4, indicating that cable formation does not require specific biochemical interactions with mucins (*63*, *67*, *68*). A three-dimensional (3D) reconstruction of the final colony is shown in Fig. 1D, illustrating that the transverse cross section of each cable has multiple cells packed side-by-side, all nematically aligned along their long axis. This network of cables extends into the bulk of the sample away from the solid boundaries, and similar cable morphologies arise for continuously rotated samples for which cells do not settle, but remain in the bulk (fig. S7)—indicating that cable formation is not strongly influenced by the presence of boundaries in the experiments.

To further test the generality of cable formation, we repeat this experiment, but using an even broader range of different polymers: PEO of three different molecular weights; Ficoll, a highly branched, uncharged polysaccharide; and sodium carboxymethyl cellulose (NaCMC), a linear, anionic polysaccharide. In all cases, we observe cable formation when the polymer solution is sufficiently concentrated, as exemplified by Fig. 1 (E and F) and movies S5 and S6. Thus, cable formation arises independent of variations in polymer chemistry, molecular weight, molecular architecture, and charge. As a final test of the generality of this phenomenon, we perform the same experiment using nonmotile strains of two other species of bacteria that also inhabit polymeric environments: *Vibrio cholerae*, a gut pathogen, and *Pseudomonas aeruginosa*, a lung pathogen. We

again observe cable formation in both cases (Fig. 2), indicating that this phenomenon arises across different cell types. Together, these results demonstrate that nonmotile bacterial colonies proliferating in sufficiently concentrated polymer solutions generically form large, serpentine, multicellular cables.

Polymer-induced entropic attraction between cells is required for cable formation

Why do cables form? Given that cable formation does not require specific biochemical interactions, we hypothesize that it instead arises from some other physicochemical influence of polymers on cells. For example, could it be that when polymers are sufficiently concentrated, they form a mesh-like network that entraps the individual cells, retaining them in the end-to-end configuration after division and thereby promoting cable formation? Our data indicate that this is not the case: Across all the different conditions tested, we find no correlation between the threshold polymer concentration at which cables begin to form and c^*, the concentration at which the different polymer molecules begin to overlap and form an interconnected network (table S1). Similarly, we find no correlation between the onset of cable formation and the solution viscosity η (table S2), indicating that cable formation does not arise solely because of the reduced ability of cells to diffusively separate from each other after division in a viscous polymer solution.

Another possibility is that the osmotic pressure Π_{osm} exerted by the polymers alters how the individual cells grow, somehow causing them to proliferate in cables. As shown in table S1, however, cable formation arises at osmotic pressures as low as about tens of pascals—far lower than the pressure at which bacterial physiology is typically altered, ~100 kPa (*69*–*75*), arguing against this possibility. Growth curves measured for shaken cultures show no appreciable differences upon polymer addition (fig. S8). Moreover, the osmotic pressure at which cables begin to form varies across different polymers (table S1), indicating that osmotic pressure does not solely control cable formation.

However, the osmotic pressure of a polymer solution can influence proliferating cells in another way: by inducing attractive interactions between them. Consider two microscale particles—e.g., adjacent cells (green in Fig. 3A)—in a polymer solution (pink). The centers of the surrounding polymer chains are excluded from a small region surrounding each particle (light gray), referred to as its excluded volume. When the particles are close enough to each other, their excluded volumes overlap and surrounding polymers are depleted from this overlapping region of volume V_{ev} (dark gray). This depletion of polymers gives rise to an osmotic pressure difference Π_{osm} across the particles, pushing them together, as schematized in Fig. 3A(i). It is well documented in colloidal science that this entropic effect forces passive, nonproliferating particles to stick together, and can be modeled as an attractive "depletion" interaction between pairs of particles. The magnitude of this depletion interaction energy is $U_{dep} = \Pi_{osm} V_{ev}$ (*76*, *77*), where Π_{osm} is determined by the polymer size and concentration (*78*) and V_{ev} is also determined by the polymer size and concentration, as well as the particle sizes, shapes, and orientations (*79*). (When the polymer can adsorb to the surface of the particles, such as in the case of mucins, the particle size is slightly enlarged by the adsorbed surface layer.) Could this polymer-induced depletion attraction between cells somehow cause them to proliferate in cables?

One way to test this idea is to examine the reversibility of cable formation: Given the entropic nature of the depletion attraction, we

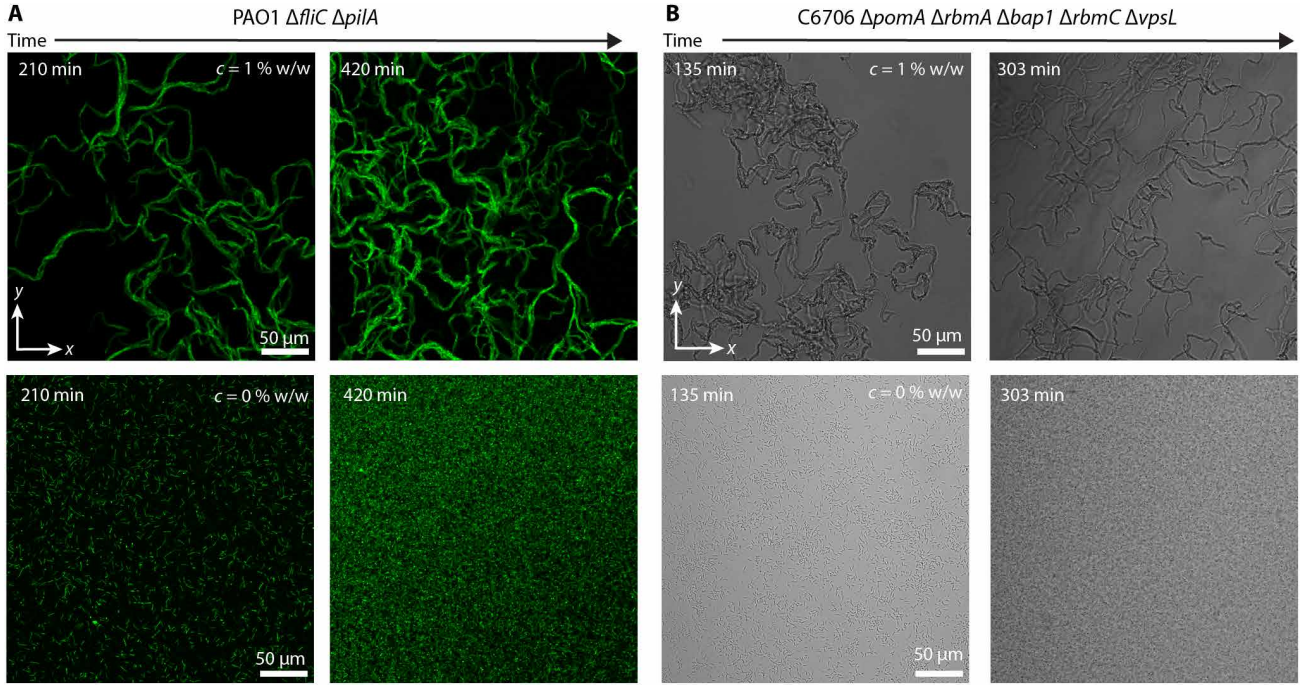

Fig. 2. Nonmotile *P. aeruginosa* and *V. cholerae* form cables as they proliferate in polymer solutions. (**A**) Time sequence of nonmotile *P. aeruginosa* proliferating in nutrient-rich fluid with (top) or without (bottom) 1% w/w PEO 1 MDa. (**B**) Same as in (A) but with nonmotile *V. cholerae*. The time indicates the duration elapsed after the 96-well plate containing the samples is inserted into the static incubator. The images were taken at different positions of the same well at the different time points.

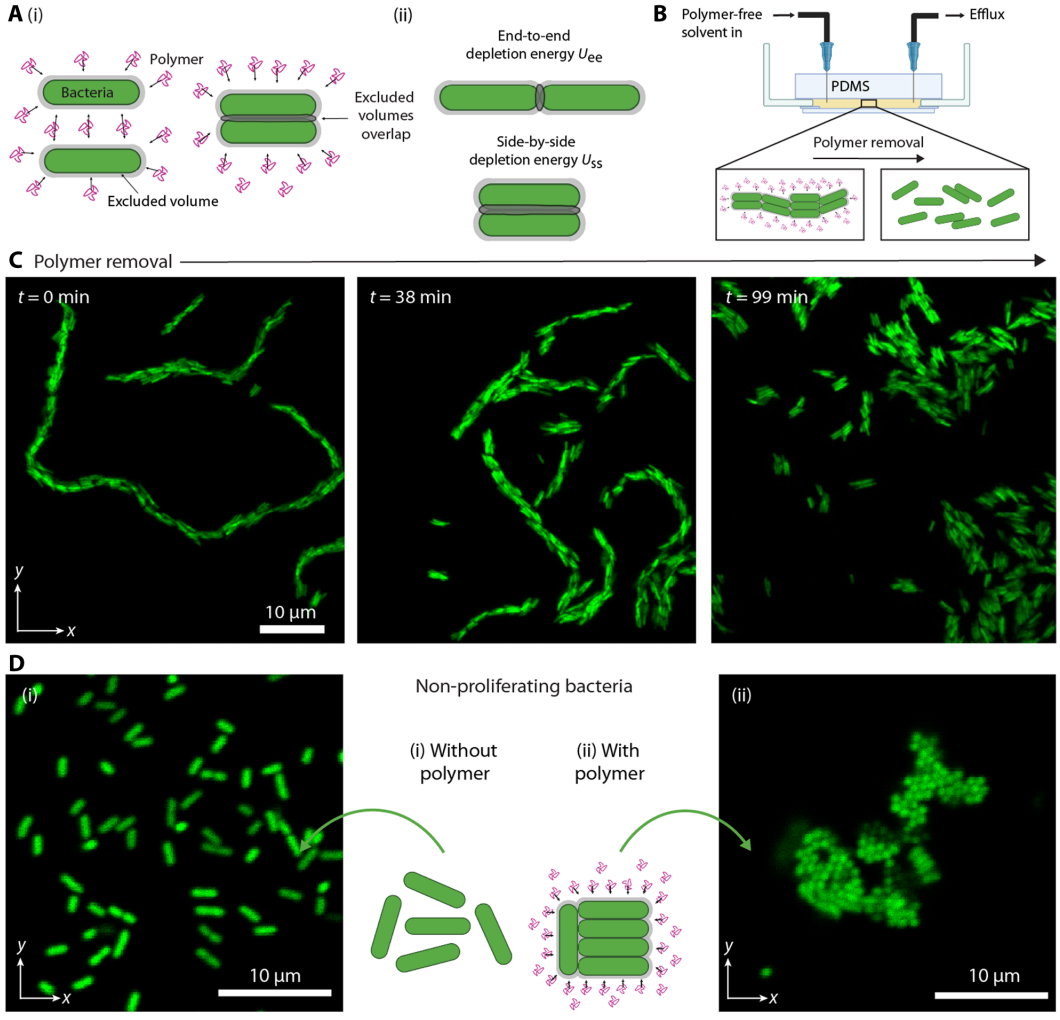

Fig. 3. Polymer-induced entropic attraction between cells is required for cable formation. (**A**) (i) Schematic of polymer (pink)–induced attraction between cells (green); the shaded gray regions show the excluded volume around each cell that is inaccessible to the centers of the polymer chains. As cells approach each other, their excluded volumes overlap (dark shaded regions), causing polymer to be depleted from the interstitial space. The osmotic pressure exerted by the surrounding polymers (arrows) drives the cells together, thereby resulting in attraction between cells. (ii) The overlapping excluded volume, and therefore the magnitude of the depletion interaction potential, is smaller for cells arranged end-to-end (top) versus side-by-side (bottom). (**B**) Schematic of experiments in which *E. coli* cables formed in polymeric fluid are gently flushed with polymer-free fluid. (**C**) Time sequence showing *E. coli* cables disintegrating when polymers are removed from their surroundings; polymer-free solvent is introduced at $t = 0$. The cells still appear to be held together in smaller side-by-side aggregates after polymer removal, likely due to the influence of other weak attractive interactions between the cells, such as those imparted by surface adhesins (*107*, *108*), that can arise after the cells are initially brought together by the polymer-induced depletion interaction. Full dynamics can be seen in movie S7. (**D**) Nonproliferating cells of *E. coli* (i) remain as a random dispersion in polymer-free fluid but (ii) aggregate side-by-side upon addition of PEO 100 kDa (0.1% w/w). Micrograph shows cells end-on, revealing the hexagonal symmetry of the side-by-side stacks.

expect that after a cable has formed, removing polymer from the solution around it should allow the cable to disintegrate via random thermal motion of the cells. This is precisely what we observe upon flushing a suspension of cables with polymer-free liquid (Fig. 3, B and C, and movie S7).

Support for the depletion attraction idea also comes from close inspection of the initial dynamics of cable formation. As exemplified in movie S8 and fig. S9 obtained using fast imaging, an initial "founder" cell grows and divides, giving rise to a pair of cells oriented end-to-end (fig. S9A). Next, instead of thermally diffusing apart, the cells quickly lock in side-by-side (fig. S9B). This preference for initially being arranged side-by-side versus end-to-end is directly predicted by the physics of the depletion interaction: The overlapping excluded volume V_{ev} and therefore the magnitude of the depletion potential U_{dep} are larger for a pair of cells when they are arranged side-by-side versus end-to-end (*13*, *80*), as schematized in Fig. 3A(ii). Thus, in the absence of other constraints, over timescales shorter than the cellular doubling time t_d, the polymer-induced depletion interaction causes pairs of cells to preferentially pack side-by-side. As a more direct test of this prediction, we culture cells in nutrient-free polymer solution, in which proliferation is arrested ($t_d \to \infty$). Under these conditions, the cells indeed aggregate side-by-side, consistent with previous observations (*9*, *10*, *12*), forming hexagonally ordered clusters (Fig. 3D). Taken altogether, these observations establish that depletion attraction induced by polymers plays a key role in cable formation. However, after an initial pair of

cells has packed side-by-side, subsequent divisions typically lead to a persistent end-to-end configuration—thus resulting in the growth of cables. Why do these subsequent divisions not lead to side-by-side packing? We find the answer to this question using agent-based simulations.

Agent-based simulations of a proliferating bacterial colony recapitulate cable formation in polymeric fluids

What biophysical features of proliferation in a polymer solution are essential for cable formation? We address this question using 2D agent-based Brownian dynamics simulations, detailed in the Supplementary Materials. Each simulation begins with a dilute dispersion of cells, just as in the experiments, that proliferate in a polymer solution with a prescribed polymer size, viscosity, and osmotic pressure. The simulations incorporate four key features, schematized in Fig. 4A:

1) The individual cells continually elongate exponentially, separating into two progeny after a doubling time t_d.

2) Adjacent cells have a short-ranged elastic repulsion that pushes them apart and keeps them from overlapping.

3) Cells are subject to thermal agitation and undergo both translational and rotational diffusion in the viscous polymer solution, with corresponding diffusivities that are determined by the polymer solution viscosity and cell size/shape.

4) Cells are subject to the polymer-induced depletion attraction given by the pairwise interaction potential of magnitude $U_{dep} = \Pi_{osm} V_{ev}$, where Π_{osm} is a characteristic of the polymer solution to be tested and V_{ev} is set by the polymer size and cell sizes and orientations.

Each simulation can then be parameterized by two dimensionless quantities: t_{rot} / t_d, which compares the characteristic timescale for cells to rotationally diffuse to their doubling time, and $U_{ee} / k_B T$, which compares the magnitude of the depletion potential for cells arranged in the initial end-to-end configuration after doubling [Fig. 3A(ii)] to the characteristic thermal energy $k_B T$, where k_B is Boltzmann's constant and T is temperature.

Remarkably, these four key biophysical features are sufficient to recapitulate the experimental observations. An example is shown in Fig. 4B. In the absence of the depletion interaction ($U_{ee} = 0\ k_B T$, top row), cells continually grow, divide, separate, and thermally diffuse away, forming a random dispersion as in the experiments (movie S9 and Fig. 1A). By contrast, when the polymer-induced depletion interaction is incorporated ($U_{ee} = 15.55\ k_B T$, bottom row), the cells quickly lock in side-by-side and then continue to proliferate end-to-end, forming a large, multicellular cable just as in the experiments (movie S10 and Fig. 1, B to E). While cables are initially two cells wide, sideways mergers between distinct cables (movies S2 and S4) or different segments of the same cable (movies S6 and S10) can produce even thicker cables at long times.

Simulations reveal that the depletion interaction holds cells in a metastable end-to-end state after division, causing cables to form

Having demonstrated that the simulations can recapitulate cable formation, we next use them to address the question: Why exactly does the polymer-induced depletion attraction cause cells to proliferate in cables? Close inspection of the incipient stage of cable formation provides a clue: As shown in the initial frames of Fig. 4B (bottom) and movie S10, a cable grows from an initial cluster of four cells, with two initially arranged in the energetically preferred side-by-side configuration, but with their progeny retained end-to-end in an interdigitated configuration—as exemplified by the leftmost insets in Fig. 5A. We call this configuration a "proto-cable." Given that the most energetically favorable configuration is for all cells to pack side-by-side (*13*, *80*), we hypothesize that this interdigitated end-to-end proto-cable is a metastable state, enabled by the strength of the depletion interaction, that keeps the cells kinetically trapped in a cable.

Simulations of four nonproliferating cells initially arranged both end-to-end and side-by-side, as shown by (i) in Fig. 5 (B and C), support this hypothesis. The cells quickly lock in to the interdigitated

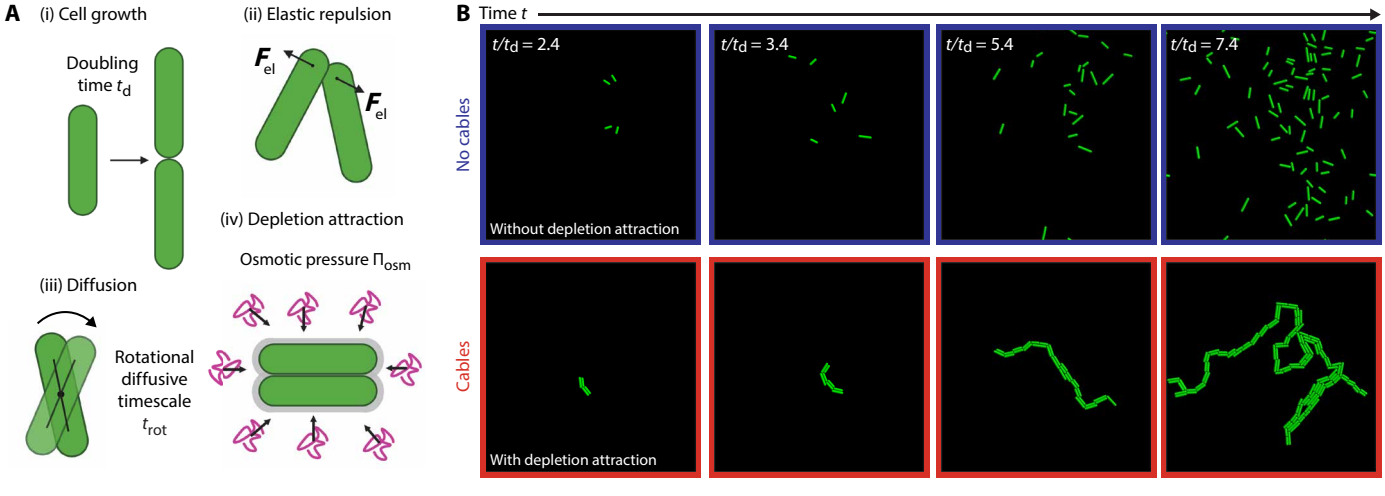

Fig. 4. Agent-based simulations recapitulate cable formation in polymeric fluids. (**A**) Schematic of the four key biophysical features incorporated into the agent-based simulations: (i) Cells are growing spherocylinders that exponentially elongate, divide, and separate, (ii) cells are stiff and elastically repel each other, (iii) cells are subject to translational and rotational diffusion due to thermal agitation, and (iv) polymers induce a depletion attraction whose interaction potential depends on the geometry and relative orientation of adjacent cells. (**B**) Time series of simulation results showing that in the polymer-free case, cells form a random dispersion, whereas with added polymer, proliferating cells form elongating cables, as in the experiments. Full dynamics can be seen in movies S9 and S10.

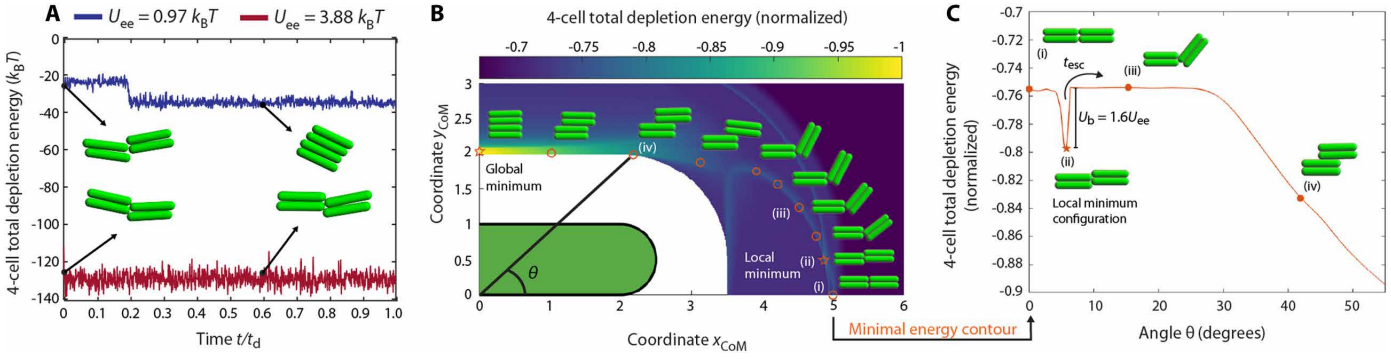

Fig. 5. The depletion interaction holds cells in a metastable end-to-end state after division. Panels show the results of model and simulations (detailed in the Supplementary Materials) of four nonproliferating cells initially arranged in a proto-cable as labeled (i) in (B) and (C). Cells quickly lock in to the interdigitated configuration labeled (ii). (**A**) When the depletion attraction is strong (red), cells remain in this interdigitated configuration, whereas when the depletion attraction is weaker (blue), cells transition to the most energetically preferred side-by-side configuration. Curves show the time series of the depletion potential, given by minus the product of the osmotic pressure and the overlapping excluded volume of a given configuration; the negative sign indicates an attractive interaction. (**B**) Color map shows the landscape of the maximum possible depletion potential between four cells in different orientations for the case of $U_{ee} = 0.97 k_BT$. Two cells are fixed in the side-by-side configuration oriented along the *x* axis, with their diameters spanning $0 < y_{CoM} < 1$ and $1 < y_{CoM} < 2$. The x_{CoM} and y_{CoM} coordinates describe the center of mass of the other two cells that can translate and rotate, again in the side-by-side configuration. The insets show 10 distinct configurations at (x_{CoM}, y_{CoM}) positions indicated by the open symbols; stars indicate minima in the energy landscape. (**C**) Minimal free-energy contour from (B), showing that the interdigitated end-to-end configuration (ii) is a metastable state characterized by a local free-energy minimum given by $U_b = 1.6U_{ee}$.

proto-cable configuration shown by (ii) in Fig. 5 (B and C). Then, if the depletion interaction is strong ($U_{ee} = 3.88\ k_BT$, red curve in Fig. 5A), the cells remain trapped in this configuration over the entire duration of the doubling t_d—ultimately enabling them to proliferate into a cable. However, when the depletion interaction is weaker ($U_{ee} = 0.97\ k_BT$), thermal diffusion allows the cells to eventually reconfigure into the most energetically favorable side-by-side configuration before they double, as shown by the abrupt dip in the blue curve. These observations suggest that the interdigitated end-to-end configuration is indeed a metastable state.

Mapping the full orientation-dependent landscape of the potential due to the depletion interaction (magnitude $U_{dep} = \Pi_{osm} V_{ev}$), indicated by the colors in Fig. 5B, confirms this suggestion. As expected, having all four cells arranged side-by-side is the most energetically favorable state, reflected by the global minimum in the free-energy landscape (leftmost star). However, as we hypothesized, the interdigitated end-to-end proto-cable configuration is a local minimum in this free-energy landscape (rightmost star). Plotting the contour of minimal energy that extends across this landscape (Fig. 5C) reveals this local minimum, of depth $\approx 1.6U_{ee}$, even more clearly.

A morphological state diagram unifies the interplay between depletion attraction and thermal diffusion in controlling cable formation

A clear picture of the biophysical rules underlying cable formation thereby emerges: After a side-by-side pair of cells divides end-to-end, shown by (i) in Fig. 5C, they remain kinetically trapped in the metastable interdigitated end-to-end proto-cable configuration (ii) for an approximate escape time t_{esc}, which is determined by cell size and shape and polymer size, concentration, osmotic pressure, and viscosity. If $t_{esc} > t_d$, the cells continue to proliferate in this configuration, ultimately generating a cable. If $t_{esc} < t_d$, however, thermal energy enables the cells to escape this kinetic trap and continue to explore other configurations, as shown by (iii) and (iv), and they do not form cables. This biophysical picture unifies all our experimental observations demonstrating that cable formation arises for diverse cell types, and across diverse polymer solutions when they are sufficiently concentrated, in a reversible manner.

As a final quantitative test of this picture, we directly compute t_{esc} for different polymer solutions. Specifically, we use our simulations to estimate the depth and curvature of the local minimum in the free-energy landscape, which corresponds to the interdigitated end-to-end proto-cable configuration, along the minimal energy contour shown in Fig. 5C. We then follow Kramers' seminal work on thermally activated escape from a potential well (*81*) to directly relate these quantities—which depend on the cell and polymer properties, as detailed in the Supplementary Materials—to the escape time. The boundary corresponding to $t_{esc} = t_d$, which separates the two different regimes predicted by our analysis, is then given by the solid black curve in Fig. 6A. This plot represents a morphological state diagram spanned by the two dimensionless control parameters revealed by our analysis, t_{rot}/t_d and U_{ee}/k_BT; to the right of the black boundary, we expect that cells proliferate into cables (red-outlined panels in Fig. 6B), whereas to the left of it, they do not (blue-outlined panels). We also expect a transitional regime immediately to the left of the black boundary, for which $t_{esc} < t_d$ and cells are not kinetically trapped in the end-to-end configuration as they double, but $U_{ss} > k_BT$, causing cells to still stack side-by-side in small aggregates (light blue). We also expect that cable formation competes with aggregation when the starting inoculum of cells is sufficiently concentrated, as described further in the Supplementary Materials. As summarized by the triangles (experiments) and circles (simulations) in Fig. 6A, with representative colony morphologies shown in Fig. 6B, our data fully confirm these expectations. Thus, taken altogether, our experiments, simulations, and theoretical analysis establish biophysical principles that describe how bacterial colonies proliferate in polymeric solutions—across diverse cell types and polymers, both natural and synthetic.

DISCUSSION

Despite their prevalence in natural habitats, little is known about how polymers influence one of the most fundamental aspects of

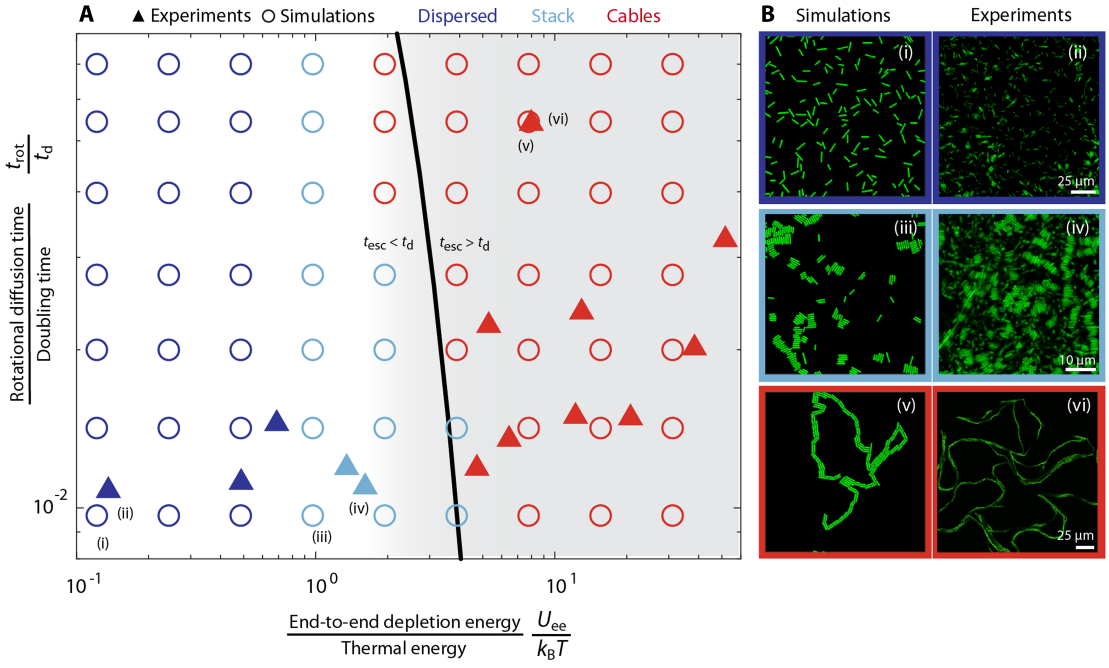

Fig. 6. A morphological state diagram unifies the interplay between depletion attraction and thermal diffusion in controlling cable formation. (**A**) State diagram is spanned by the two dimensionless parameters t_{rot} / t_d and U_{ee} / k_BT, where the former compares the characteristic timescale for cells to rotationally diffuse to their doubling time, and the latter compares the magnitude of the depletion potential for cells arranged in the end-to-end configuration to the thermal energy; both are calculated as described in the Supplementary Materials. Filled triangles and open circles show experimental and simulation results, respectively. Solid black curve shows our theoretical prediction for the onset of cable formation, given by $t_{esc} = t_d$, where t_{esc} is the typical duration spent in the metastable interdigitated end-to-end configuration (given by eq. S46) and t_d is the doubling time. Both agent-based simulation and t_{esc} shown in this figure assume a polymer radius of 75 nm, approximately characteristic of that used in the experiments. The shaded gray region indicates our estimate for the region of this state diagram that describes in situ host mucus (detailed in the Supplementary Materials); interestingly, this region coincides with the onset of cable formation. Dark blue, light blue, and red symbols indicate colonies that formed random dispersions, small side-by-side stacks, and cables, respectively. (**B**) Snapshots of representative colony morphologies for each of these three states. (i) $U_{ee} = 0.25\ k_BT$, $t_{rot} = 0.009\ t_d$; (ii) 0.01% w/w Ficoll 400 kDa; (iii) $U_{ee} = 0.97\ k_BT$, $t_{rot} = 0.009\ t_d$; (iv) 0.01% w/w NaCMC 250 kDa; (v) $U_{ee} = 7.77\ k_BT$, $t_{rot} = 0.05\ t_d$; (vi) 0.25% w/w PEO 5 MDa.

bacterial life—their proliferation in colonies. By combining experiments, simulations, and theory, we have shown that extracellular polymers can shape bacterial colonies through purely physicochemical interactions, as broadly suggested by previous simulations (*82*). In particular, we found that nonmotile bacteria proliferating in sufficiently concentrated polymer solutions—both biological and synthetic—nematically align to form an intertwined network of long, serpentine, multicellular cables. This characteristic colony morphology arises due to the combined influence of polymer-induced entropic attraction holding cells together and the enhanced solution viscosity hindering cells from diffusively separating after dividing. Hence, this phenomenon arises generically and predictably across diverse bacterial species and polymer compositions; indeed, not only did our experiments directly demonstrate cable formation in gut mucus, but also our analysis (detailed in the Supplementary Materials) indicates that, more broadly, biological polymers like mucus have physicochemical properties that promote cable formation, as shown by the gray region of Fig. 6. Our work thus uncovers quantitative principles governing the morphogenesis of bacterial colonies—and potentially other microbial systems—in their complex environments in the real world. It also opens up a new direction for research in soft matter physics: While polymer-induced entropic attraction is well studied for passive particulate systems, our work builds on previous simulations of biofilms (*82*) to highlight that fascinating new behaviors can emerge when the constituent particulates can also proliferate (*15*). Cable-like structures with smectic, i.e., layered, internal ordering have been observed in systems of passive nanorods under strong depletion attraction (*83*); however, in the bacterial cables reported here, while there appears to be a slight amount of such ordering (e.g., in Fig. 1D), we have not observed appreciable smectic ordering over large scales—possibly because it is disrupted by the natural variability in cellular lengths within a cable. Whether such ordering may arise during cable growth under other conditions, such as those induced by nutrient starvation (*84*), will be interesting to investigate in the future. Another interesting direction for future research will be to explore the generality of cable formation in complex environments with nonpolymeric depletants, as described further in the Supplementary Materials.

Colony morphologies reminiscent of cables—often called "chains" or "cords"—have been previously observed in a variety of bacterial systems. However, their origin is likely fundamentally different from the cables reported here; while cables arise generically due to entropic forces induced by polymers on cells, chains/cords are thought to form instead due to specific biochemical interactions or cellular processes. One prominent example arises when host-secreted antibodies cross-link proliferating cells of *Salmonella enterica* together (*85*). Another example is thought to arise for *Mycobacterium tuberculosis* due to hydrophobic interactions between mycomembrane lipids that

strongly adhere cells together (*86*); cell surface hydrophobicity can similarly mediate aggregate formation in *P. aeruginosa* during pathogenesis (*87*). Similarly, under certain conditions, *E. coli* surface adhesins can adhere cells together in chains during biofilm formation (*88*). In all three of these cases, specific biochemical interactions prevent cells from separating after division—unlike in cable formation, which arises due to a fundamentally different physicochemical mechanism across a broad range of polymer chemistries. A useful direction for future work will be to investigate how cable formation may be altered by the added influence of such specific biochemical interactions. A final example is the chains of cells that arise during *Bacillus subtilis* biofilm formation; unlike our cables, in which cells fully divide and separate from each other during proliferation, these chains form because cells do not completely divide and separate, and are therefore inseparably retained end-to-end (*89*–*91*). Our work thus reveals a distinct, more general mechanism by which proliferating bacteria can form such long, multicellular cables upon exposure to polymers.

Extensive work has focused on the ability of polymers to enhance the mobility of swimming bacteria (*5*–*8*). By contrast, their influence on nonmotile cells is understudied, despite the fact that many bacteria in natural polymeric environments (e.g., mucus) are nonmotile or lose motility (*33*–*56*)—an important virulence factor that often correlates with pathogenesis and colonization/biofilm formation. Our study therefore focused on the proliferation of nonmotile cells. However, a natural extension of our work is to investigate how cellular motility may alter cable formation. Cables are not formed when we repeat our experiments with swimming *E. coli* (movies S11 and S12)—presumably because the hydrodynamic force generated by swimming cells exceeds the attractive depletion force induced by polymers, as supported by calculations in the Supplementary Materials (*12*, *92*). Moreover, in the case of mucus, additional biochemical interactions can further promote dispersal of swimming cells (*93*). Further investigating the interplay between cellular motility and polymer-induced cable formation will thus be an interesting direction for future research. Also, given that the entropic forces underlying cable formation depend sensitively on cell size and shape, another natural extension of our work is to investigate how cables form for cells of other shapes (e.g., curved) and in mixtures of different founder cell types. Our study also focused on cable formation by non–biofilm-forming strains of bacteria when exposed to exogenous polymers. Another interesting direction for future research is to investigate how cable formation may be altered in the case of biofilm formers; it may even be possible that the polymeric EPS secreted by the cells drives cable formation on its own, without requiring exposure to exogenous polymers.

What are the biological implications of cable formation? This phenomenon could be beneficial to nonmotile bacteria by giving their colonies a way to extend outward and explore new environmental niches, including on surfaces or within host tissues (*86*, *94*). Proliferating in a cable could also help bacteria counter host immune responses against them, either mechanically by impeding phagocytosis (*95*) and compressing host cell structures (*86*) or geometrically by reducing the amount of cell surface that is exposed to the surroundings—compared to the case of freely dispersed cells—potentially helping to protect cells within a cable from antimicrobials (*86*). Alternatively, it could be that hosts secrete polymers, such as mucins, to force cells to proliferate in cables, potentially enhancing clonal extinction rates and pathogen clearance (*85*), in addition to specific biochemical interactions that down-regulate pathogenic genes (*1*, *64*, *96*). Such effects may also be induced by dietary polymers transiting through the gut (*97*, *98*), potentially providing an indirect link between host diet, the physiology of the gut microbiome, and host health. Moreover, by localizing cells together, cable formation could alter the dynamics and extent of infection by bacteriophages throughout a colony, as suggested by simulations (*99*). Building on our findings to investigate these possible consequences of cable formation will be an exciting direction for future research.

METHODS

Preparation of cells

E. coli

We incubate an overnight culture of *E. coli* strain W3110 in 2% w/w Lennox Lysogeny Broth (LB) at 30°C. Next, we inoculate 20 μl from the overnight culture in 2 ml of 2% w/w LB for 3 hours such that, at the time of imaging, bacteria are in mid-exponential phase. We use a strain with a deletion of the flagellar regulatory gene *flhDC* that renders the cells nonmotile; we verify that these cells are nonmotile using direct visualization. This strain likely does not form biofilms for two reasons: first, because it is deficient in the production of cellulose, a key component of the biofilm extracellular matrix (*100*, *101*), and second, because it only produces curli fibers—another key component of the biofilm extracellular matrix—under nutrient starvation conditions (*102*, *103*), whereas our experiments are performed in nutrient-rich conditions.

P. aeruginosa

We incubate an overnight culture of *P. aeruginosa* strain PA01 in 2% w/w LB, supplemented with carbenicillin (200 μg/ml) to preserve the strain's fluorescence, at 37°C. Next, we inoculate 20 μl from the overnight culture in 2 ml of 2% w/w LB for 3 hours. We use a strain with a double *fliC* and *pilA* deletion that renders the cells nonmotile; we verify that these cells are nonmotile using direct visualization. This strain likely does not form biofilms because it lacks both pili and flagella, which are key factors in biofilm formation (*104*–*106*).

V. cholerae

We incubate an overnight culture of *V. cholerae* O1 biovar El Tor strain C6706 in 2% w/w LB at 37 °C. Next, we inoculate 20 μl from the overnight culture in 2 ml of 2% w/w LB for 5 hours with the addition of rolling beads in culture to keep the bacteria dispersed. We use a strain with several gene deletions: It has a deletion of *pomA*, which renders the cells nonmotile; we verify that these cells are nonmotile using direct visualization. It also has deletions of *rbmA*, *bap1*, *rbmC*, and *vpsL*, which renders the cells as nonbiofilm formers.

Preparation of polymer solutions

Synthetic polymers

We obtain PEO 5 MDa from ColorCon and Sigma-Aldrich, PEO 1 MDa and 100 kDa from ColorCon, Ficoll 400 kDa from Research Products International, and Carboxymethyl Cellulose Sodium Salt from MP Biomedicals. We prepare polymer stock solutions in 2% w/w LB and then put them on a spinning rotor for at least 8 hours until the solution is optically clear. The PEO solutions are additionally filtered using a 5-μm pore size membrane from GE Healthcare Life Sciences. We use dilutions of these concentrated stock solutions in LB to prepare polymer solutions at defined concentrations.

Human colonic mucus

We use mucus from human primary transverse colon cells (*57*) obtained from Altis Biosystems. In particular, the mucus is siphoned

from the surface of a culture of resident goblet cells (Altis RepliGut Planar transverse colon model), and then directly frozen and stored at −20°C. We then defrost and mix this mucus stock solution with 10% w/w LB at an appropriate ratio such that the final LB concentration is 2% w/w and the final mucus concentration is 0.5% w/w.

Muc2 mucins

We use purified native porcine gel-forming intestinal mucin (Muc2) (*1*, *2*) obtained from the Ribbeck laboratory at Massachusetts Institute of Technology as a lyophilized powder. This powder is dissolved in autoclaved distilled water at a stock concentration of 1% w/w. We then leave this solution on a spinning rotor at 4°C overnight a day before using it in an experiment. The day of the experiment, we mix the Muc2 stock solution with 10% w/w LB and use dilutions with autoclaved distilled water such that the final LB concentration is 2% w/w and the final Muc2 concentration is 0.5% w/w. We then leave the test solution on a spinning rotor for at least 2 hours before use in the experiment to ensure a homogeneous solution.

Imaging bacterial proliferation

E. coli in synthetic polymer solutions

We fill the base (20 mm diameter, ~1 mm height) of a transparent-walled glass-bottom petri dish, 35 mm in diameter and 10 mm in height overall, with a test solution containing cells at an initial concentration of $\approx 4 \times 10^5$ cells/ml and polymer at the concentration to be tested. Next, we seal this base with an overlying circular polydimethylsiloxane (PDMS) slab to minimize evaporation while still allowing oxygen to be available. We then image the sealed chamber from below using a Nikon A1R+ inverted laser scanning confocal microscope with the stage maintained at 30 ± 1°C. We acquire fluorescent optical slices throughout the depth of the sample every 1 to 5 min over a total duration of ≈6 to 14 hours.

For the experiment in Fig. 3 (B and C) investigating the reversibility of cable formation, we again use a transparent-walled glass-bottom petri dish sealed with an overlying PDMS slab as described above. However, we additionally pierce the PDMS slab with three 20-gauge needles, sealed using optical glue, and connected to a Harvard Apparatus 11 Elite syringe pump to provide fluid in/outflow. In particular, one needle acts as an inlet for injection of the test solution containing $\approx 4 \times 10^5$ cells/ml suspended in 0.1% w/w PEO 100 kDa as the polymer; the second acts as an inlet for injection of polymer-free LB media; and the third acts as the outlet. We then image the sealed chamber from below using a Nikon A1R+ inverted laser scanning confocal microscope with the stage maintained at 30 ± 1°C as before, first under quiescent no-flow conditions with the chamber filled with the test solution containing cells and polymer. Once cables have formed, we then pump polymer-free fluid through at a flow rate of 5 μl/min to remove polymer-containing solution. Our experiments shown in movie S13 (snapshots in fig. S10) indicate that these flow rates are insufficient to fragment cables due to hydrodynamic forces.

For the experiment in Fig. 3D using nonproliferating cells, we inoculate 20 μl from an overnight culture of cells into 2 ml of 2% w/w LB and let the bacteria grow for 3 hours in a shaking incubator until they reach mid-exponential phase. We then mix 10 μl of the culture with a solution of PEO 100 kDa dissolved in 1× Difco M9 Minimal Salts without a nutrient source at a polymer concentration of 0.1% w/w and a cellular concentration of $\approx 6 \times 10^7$ cells/ml. We then again fill the base of a transparent-walled glass-bottom petri dish with the solution, sealed with an overlying PDMS slab as described above, and incubate the dish at 30°C in a static incubator for 2 hours. We then image the sealed chamber from below using a Nikon A1R+ inverted laser scanning confocal microscope with the stage maintained at 30 ± 1°C.

E. coli in human colonic mucus

We fill a custom-made PDMS rectangular channel (22 mm long, 2 mm wide, 25 or 90 μm high) with the test mucus solution containing cells at an initial concentration of $\sim 3 \times 10^6$ cells/ml. We then image the sealed channel from below using a Nikon A1R+ inverted laser scanning confocal microscope with the stage maintained at 33 ± 1°C. We acquire fluorescent optical slices throughout the depth of the sample every 3 min over a total duration of ≈12 hours.

E. coli in Muc2 solutions

We fill a glass capillary (4 cm long, 5 mm wide, 500 μm high) with the test Muc2 solution containing cells at an initial concentration of $\sim 3 \times 10^5$ cells/ml. We then image the capillary, sealed on both ends with paraffin oil to minimize evaporation while still allowing oxygen to be available, from below using a Nikon A1R+ inverted laser scanning confocal microscope with the stage maintained at 30 ± 1°C. We acquire fluorescent optical slices throughout the depth of the sample every 3 min over a total duration of ≈12 hours.

P. aeruginosa and V. cholerae in polymer solutions

We fill individual wells of a glass-bottom 96-well plate with 200 μl of a test polymer solution and 0.2 μl of the inoculum of cells such that their initial concentration is $\sim 3 \times 10^6$ to 6×10^6 cells/ml. We store the plate in a static 37°C incubator and image the plate at different time points: For *P. aeruginosa*, we image at 210 and 420 min after the start of incubation, and for *V. cholerae*, we image at 135 and 303 min after incubation as shown in Fig. 2. For all images taken, we use a 20× air objective mounted in a Nikon A1R+ inverted laser scanning confocal microscope with the stage maintained at 37 ± 1°C.

Supplementary Materials

The PDF file includes:

Supplementary Text
Figs. S1 to S10
Tables S1 to S3
Legends for movies S1 to S13

Other Supplementary Material for this manuscript includes the following:

Movies S1 to S13

REFERENCES AND NOTES

1. B. X. Wang, C. M. Wu, K. Ribbeck, Home, sweet home: How mucus accommodates our microbiota. *FEBS J.* **288**, 1789–1799 (2021).
2. A. McShane, J. Bath, A. M. Jaramillo, C. Ridley, A. A. Walsh, C. M. Evans, D. J. Thornton, K. Ribbeck, Mucus. *Curr. Biol.* **31**, R938–R945 (2021).
3. A. W. Decho, T. Gutierrez, Microbial extracellular polymeric substances (EPSs) in ocean systems. *Front. Microbiol.* **8**, 922 (2017).
4. W. Yin, Y. Wang, L. Liu, J. He, Biofilms: The microbial "Protective Clothing" in extreme environments. *Int. J. Mol. Sci.* **20**, 3423 (2019).
5. A. Martínez-Calvo, C. Trenado-Yuste, S. S. Datta, "Active transport in complex environments" in *Out-of-Equilibrium Soft Matter* (The Royal Society of Chemistry, 2021).
6. A. E. Patteson, A. Gopinath, M. Goulian, P. E. Arratia, Running and tumbling with *E. coli* in polymeric solutions. *Sci. Rep.* **5**, 15761 (2015).
7. V. A. Martinez, J. Schwarz-Linek, M. Reufer, L. G. Wilson, A. N. Morozov, W. C. K. Poon, Flagellated bacterial motility in polymer solutions. *Proc. Natl. Acad. Sci. U.S.A.* **111**, 17771–17776 (2014).
8. A. Zöttl, J. M. Yeomans, Enhanced bacterial swimming speeds in macromolecular polymer solutions. *Nat. Phys.* **15**, 554–558 (2019).

9. P. R. Secor, L. A. Michaels, A. Ratjen, L. K. Jennings, P. K. Singh, Entropically driven aggregation of bacteria by host polymers promotes antibiotic tolerance in Pseudomonas aeruginosa. *Proc. Natl. Acad. Sci. U.S.A.* **115**, 10780–10785 (2018).
10. G. Dorken, G. P. Ferguson, C. E. French, W. C. K. Poon, Aggregation by depletion attraction in cultures of bacteria producing exopolysaccharide. *J. R. Soc. Interface* **9**, 3490–3502 (2012).
11. K. E. Eboigbodin, J. R. A. Newton, A. F. Routh, C. A. Biggs, Role of nonadsorbing polymers in bacterial aggregation. *Langmuir* **21**, 12315–12319 (2005).
12. M. K. Porter, A. Preska Steinberg, R. F. Ismagilov, Interplay of motility and polymer-driven depletion forces in the initial stages of bacterial aggregation. *Soft Matter* **15**, 7071–7079 (2019).
13. P. R. Secor, L. A. Michaels, D. A. C. Bublitz, L. K. Jennings, P. K. Singh, The depletion mechanism actuates bacterial aggregation by exopolysaccharides and determines species distribution & composition in bacterial aggregates. *Front. Cell. Infect. Microbiol.* **12**, 869736 (2022).
14. J. A. Shapiro, Bacteria as multicellular organisms. *Sci. Am.* **258**, 82–89 (1988).
15. O. Hallatschek, S. S. Datta, K. Drescher, J. Dunkel, J. Elgeti, B. Waclaw, N. S. Wingreen, Proliferating active matter. *Nat. Rev. Phys.* **5**, 407–419 (2023).
16. C. Fei, S. Mao, J. Yan, R. Alert, H. A. Stone, B. L. Bassler, N. S. Wingreen, A. Košmrlj, Nonuniform growth and surface friction determine bacterial biofilm morphology on soft substrates. *Proc. Natl. Acad. Sci. U.S.A.* **117**, 7622–7632 (2020).
17. M. Trejo, C. Douarche, V. Bailleux, C. Poulard, S. Mariot, C. Regeard, E. Raspaud, Elasticity and wrinkled morphology of *Bacillus subtilis* pellicles. *Proc. Natl. Acad. Sci. U.S.A.* **110**, 2011–2016 (2013).
18. A. Martínez-Calvo, T. Bhattacharjee, R. K. Bay, H. N. Luu, A. M. Hancock, N. S. Wingreen, S. S. Datta, Morphological instability and roughening of growing 3D bacterial colonies. *Proc. Natl. Acad. Sci. U.S.A.* **119**, e2208019119 (2022).
19. H. Fujikawa, M. Matsushita, Fractal growth of *Bacillus subtilis* on agar plates. *J. Phys. Soc. Jpn.* **58**, 3875–3878 (1989).
20. F. D. C. Farrell, O. Hallatschek, D. Marenduzzo, B. Waclaw, Mechanically driven growth of quasi-two-dimensional microbial colonies. *Phys. Rev. Lett.* **111**, 168101 (2013).
21. E. Ben-Jacob, O. Schochet, A. Tenenbaum, I. Cohen, A. Czirók, T. Vicsek, Generic modelling of cooperative growth patterns in bacterial colonies. *Nature* **368**, 46–49 (1994).
22. M. Matsushita, J. Wakita, H. Itoh, I. Ràfols, T. Matsuyama, H. Sakaguchi, M. Mimura, Interface growth and pattern formation in bacterial colonies. *Phys. A. Stat. Mech. Appl.* **249**, 517–524 (1998).
23. E. Ben-Jacob, I. Cohen, H. Levine, Cooperative self-organization of microorganisms. *Adv. Phys.* **49**, 395–554 (2000).
24. A. Seminara, T. E. Angelini, J. N. Wilking, H. Vlamakis, S. Ebrahim, R. Kolter, D. A. Weitz, M. P. Brenner, Osmotic spreading of Bacillus subtilis biofilms driven by an extracellular matrix. *Proc. Natl. Acad. Sci. U.S.A.* **109**, 1116–1121 (2012).
25. L. Xiong, Y. Cao, R. Cooper, W. J. Rappel, J. Hasty, L. Tsimring, Flower-like patterns in multi-species bacterial colonies. *eLife* **9**, e48885 (2020).
26. B. Bottura, L. M. Rooney, P. A. Hoskisson, G. McConnell, Intra-colony channel morphology in *Escherichia coli* biofilms is governed by nutrient availability and substrate stiffness. *Biofilm* **4**, 100084 (2022).
27. O. Hallatschek, P. Hersen, S. Ramanathan, D. R. Nelson, Genetic drift at expanding frontiers promotes gene segregation. *Proc. Natl. Acad. Sci. U.S.A.* **104**, 19926–19930 (2007).
28. M. J. I. Müller, B. I. Neugeboren, D. R. Nelson, A. W. Murray, Genetic drift opposes mutualism during spatial population expansion. *Proc. Natl. Acad. Sci. U.S.A.* **111**, 1037–1042 (2014).
29. C. D. Nadell, K. Drescher, K. R. Foster, Spatial structure, cooperation and competition in biofilms. *Nat. Rev. Microbiol.* **14**, 589–600 (2016).
30. F. D. Farrell, M. Gralka, O. Hallatschek, B. Waclaw, Mechanical interactions in bacterial colonies and the surfing probability of beneficial mutations. *J. R. Soc. Interface* **14**, 20170073 (2017).
31. M. Whiteley, M. G. Bangera, R. E. Bumgarner, M. R. Parsek, G. M. Teitzel, S. Lory, E. P. Greenberg, Gene expression in *Pseudomonas aeruginosa* biofilms. *Nature* **413**, 860–864 (2001).
32. T.-F. Mah, B. Pitts, B. Pellock, G. C. Walker, P. S. Stewart, G. A. O'Toole, A genetic basis for *Pseudomonas aeruginosa* biofilm antibiotic resistance. *Nature* **426**, 306–310 (2003).
33. A. Folkesson, L. Jelsbak, L. Yang, H. K. Johansen, O. Ciofu, N. Høiby, S. Molin, Adaptation of Pseudomonas aeruginosa to the cystic fibrosis airway: An evolutionary perspective. *Nat. Rev. Microbiol.* **10**, 841–851 (2012).
34. M. H. Rau, S. K. Hansen, H. K. Johansen, L. E. Thomsen, C. T. Workman, K. F. Nielsen, L. Jelsbak, N. Høiby, L. Yang, S. Molin, Early adaptive developments of *Pseudomonas aeruginosa* after the transition from life in the environment to persistent colonization in the airways of human cystic fibrosis hosts. *Environ. Microbiol.* **12**, 1643–1658 (2010).
35. L. Cullen, S. McClean, Bacterial adaptation during chronic respiratory infections. *Pathogens* **4**, 66–89 (2015).
36. E. E. Smith, D. G. Buckley, Z. Wu, C. Saenphimmachak, L. R. Hoffman, D. A. D'Argenio, S. I. Miller, B. W. Ramsey, D. P. Speert, S. M. Moskowitz, J. L. Burns, R. Kaul, M. V. Olson, Genetic adaptation by Pseudomonas aeruginosa to the airways of cystic fibrosis patients. *Proc. Natl. Acad. Sci. U.S.A.* **103**, 8487–8492 (2006).
37. C. Winstanley, S. O'Brien, M. A. Brockhurst, *Pseudomonas aeruginosa* evolutionary adaptation and diversification in cystic fibrosis chronic lung infections. *Trend. Microbiol.* **24**, 327–337 (2016).
38. J. Jeukens, B. Boyle, I. Kukavica-Ibrulj, M. M. Ouellet, S. D. Aaron, S. J. Charette, J. L. Fothergill, N. P. Tucker, C. Winstanley, R. C. Levesque, Comparative genomics of isolates of a *Pseudomonas aeruginosa* epidemic strain associated with chronic lung infections of cystic fibrosis patients. *PLOS ONE* **9**, e87611 (2014).
39. E. Mahenthiralingam, M. E. Campbell, D. P. Speert, Nonmotility and phagocytic resistance of *Pseudomonas aeruginosa* isolates from chronically colonized patients with cystic fibrosis. *Infect. Immun.* **62**, 596–605 (1994).
40. E. Amiel, R. R. Lovewell, G. A. O'Toole, D. A. Hogan, B. Berwin, *Pseudomonas aeruginosa* evasion of phagocytosis is mediated by loss of swimming motility and is independent of flagellum expression. *Infect. Immun.* **78**, 2937–2945 (2010).
41. V. Balloy, A. Verma, S. Kuravi, M. Si-Tahar, M. Chignard, R. Ramphal, The role of flagellin versus motility in acute lung disease caused by Pseudomonas aeruginosa. *J. Infect. Dis.* **196**, 289–296 (2007).
42. M. A. Luzar, M. J. Thomassen, T. C. Montie, Flagella and motility alterations in *Pseudomonas aeruginosa* strains from patients with cystic fibrosis: Relationship to patient clinical condition. *Infect. Immun.* **50**, 577–582 (1985).
43. R. Okumura, T. Kurakawa, T. Nakano, H. Kayama, M. Kinoshita, D. Motooka, K. Gotoh, T. Kimura, N. Kamiyama, T. Kusu, Y. Ueda, H. Wu, H. Iijima, S. Barman, H. Osawa, H. Matsuno, J. Nishimura, Y. Ohba, S. Nakamura, T. Iida, M. Yamamoto, E. Umemoto, K. Sano, K. Takeda, Lypd8 promotes the segregation of flagellated microbiota and colonic epithelia. *Nature* **532**, 117–121 (2016).
44. T. C. Cullender, B. Chassaing, A. Janzon, K. Kumar, C. E. Muller, J. J. Werner, L. T. Angenent, M. E. Bell, A. G. Hay, D. A. Peterson, J. Walter, M. Vijay-Kumar, A. T. Gewirtz, R. E. Ley, Innate and adaptive immunity interact to quench microbiome flagellar motility in the gut. *Cell Host Microbe* **14**, 571–581 (2013).
45. J. G. Mitchell, L. Pearson, A. Bonazinga, S. Dillon, H. Khouri, R. Paxinos, Long lag times and high velocities in the motility of natural assemblages of marine bacteria. *Appl. Environ. Micobiol.* **61**, 877–882 (1995).
46. S. J. Giovannoni, H. J. Tripp, S. Givan, M. Podar, K. L. Vergin, D. Baptista, L. Bibbs, J. Eads, T. H. Richardson, M. Noordewier, M. S. Rappé, J. M. Short, J. C. Carrington, E. J. Mathur, Genome streamlining in a cosmopolitan oceanic bacterium. *Science* **309**, 1242–1245 (2005).
47. E. Rossi, M. Paroni, P. Landini, Biofilm and motility in response to environmental and host-related signals in gram negative opportunistic pathogens. *J. Appl. Micobiol.* **125**, 1587–1602 (2018).
48. T. Todhanakasem, G. M. Young, Loss of flagellum-based motility by listeria monocytogenes results in formation of hyperbiofilms. *J. Bacteriol.* **190**, 6030–6034 (2008).
49. S. Zhu, B. Gao, Bacterial flagella loss under starvation. *Trend. Microbiol.* **28**, 785–788 (2020).
50. X.-Y. Zhuang, C.-J. Lo, Construction and loss of bacterial flagellar filaments. *Biomolecules* **10**, 1528 (2020).
51. S. B. Guttenplan, D. B. Kearns, Regulation of flagellar motility during biofilm formation. *FEMS Microbiol. Rev.* **37**, 849–871 (2013).
52. F. H. Yildiz, N. A. Dolganov, G. K. Schoolnik, Vpsr, a member of the response regulators of the two-component regulatory systems, is required for expression of vps biosynthesis genes and epsetr-associated phenotypes in Vibrio cholerae o1 el tor. *J. Bacteriol.* **183**, 1716–1726 (2001).
53. K. Sauer, A. K. Camper, G. D. Ehrlich, J. W. Costerton, D. G. Davies, *Pseudomonas aeruginosa* displays multiple phenotypes during development as a biofilm. *J. Bacteriol.* **184**, 1140–1154 (2002).
54. F. H. Yildiz, X. S. Liu, A. Heydorn, G. K. Schoolnik, Molecular analysis of rugosity in a *Vibrio cholerae* O1 El tor phase variant. *Mol. Microbiol.* **53**, 497–515 (2004).
55. K. M. Blair, L. Turner, J. T. Winkelman, H. C. Berg, D. B. Kearns, A molecular clutch disables flagella in the Bacillus subtilis biofilm. *Science* **320**, 1636–1638 (2008).
56. N. Verstraeten, K. Braeken, B. Debkumari, M. Fauvart, J. Fransaer, J. Vermant, J. Michiels, Living on a surface: Swarming and biofilm formation. *Trend. Microbiol.* **16**, 496–506 (2008).
57. Y. Wang, M. DiSalvo, D. B. Gunasekara, J. Dutton, A. Proctor, M. S. Lebhar, I. A. Williamson, J. Speer, R. L. Howard, N. M. Smiddy, S. J. Bultman, C. E. Sims, S. T. Magness, N. L. Allbritton, Self-renewing monolayer of primary colonic or rectal epithelial cells. *Cell Mol. Gastroenterol. Hepatol.* **4**, 165–182.e7 (2017).
58. P. S. Cohen, J. C. Arruda, T. J. Williams, D. C. Laux, Adhesion of a human fecal Escherichia coli strain to mouse colonic mucus. *Infect. Immun.* **48**, 139–145 (1985).
59. M. Lindahl, I. Carlstedt, Binding of k99 fimbriae of enterotoxigenic Escherichia coli to pig small intestinal mucin glycopeptides. *Microbiology* **136**, 1609–1614 (1990).

60. E. M. Tuomola, A. C. Ouwehand, S. J. Salminen, The effect of probiotic bacteria on the adhesion of pathogens to human intestinal mucus. *FEMS Immun. Med. Microbiol.* **26**, 137–142 (1999).
61. T. V. Vakhrusheva, Y. P. Baikova, N. G. Balabushevich, S. A. Gusev, G. Y. Lomakina, E. A. Sholina, M. A. Moshkovskaya, P. L. Shcherbakov, O. V. Pobeguts, E. V. Mikhal'chik, Binding of mucin by *E. coli* from human gut. *Bull. Exp. Biol. Med.* **165**, 235–238 (2018).
62. T. Sauvaitre, J. van Landuyt, C. Durif, C. Roussel, A. Sivignon, S. Chalancon, O. Uriot, F. van Herreweghen, T. van de Wiele, L. Etienne-Mesmin, S. Blanquet-Diot, Role of mucus-bacteria interactions in enterotoxigenic *Escherichia coli* (etec) h10407 virulence and interplay with human microbiome. *NPJ Biofilms Microbiomes* **8**, 86 (2022).
63. C. Werlang, G. Cárcarmo-Oyarce, K. Ribbeck, Engineering mucus to study and influence the microbiome. *Nat. Rev. Mater.* **4**, 134–145 (2019).
64. K. M. Wheeler, G. Cárcamo-Oyarce, B. S. Turner, S. Dellos-Nolan, J. Y. Co, S. Lehoux, R. D. Cummings, D. J. Wozniak, K. Ribbeck, Mucin glycans attenuate the virulence of *Pseudomonas aeruginosa* in infection. *Nat. Microbiol.* **4**, 2146–2154 (2019).
65. W. A. Niu, S. L. Rivera, M. S. Siegrist, M. M. Santore, Depletion forces drive reversible capture of live bacteria on non-adhesive surfaces. *Soft Matter* **17**, 8185–8194 (2021).
66. M. Kesimer, J. K. Sheehan, Mass spectrometric analysis of mucin core proteins. *Methods Mol. Biol.* **842**, 67–79 (2012).
67. C. M. Wu, K. M. Wheeler, G. Cárcamo-Oyarce, K. Aoki, A. McShane, S. S. Datta, J. L. Mark Welch, M. Tiemeyer, A. L. Griffen, K. Ribbeck, Mucin glycans drive oral microbial community composition and function. *NPJ Biofilms Microbiomes* **9**, 11 (2023).
68. J. Takagi, K. Aoki, B. S. Turner, S. Lamont, S. Lehoux, N. Kavanaugh, M. Gulati, A. Valle Arevalo, T. J. Lawrence, C. Y. Kim, B. Bakshi, M. Ishihara, C. J. Nobile, R. D. Cummings, D. J. Wozniak, M. Tiemeyer, R. Hevey, K. Ribbeck, Mucin O-glycans are natural inhibitors of Candida albicans pathogenicity. *Nat. Chem. Biol.* **18**, 762–773 (2022).
69. S. M. Rubinstein, I. Kolodkin-Gal, A. Mcloon, L. Chai, R. Kolter, R. Losick, D. A. Weitz, Osmotic pressure can regulate matrix gene expression in *Bacillus subtilis*. *Mol. Microbiol.* **86**, 426–436 (2012).
70. R. Buda, Y. Liu, J. Yang, S. Hegde, K. Stevenson, F. Bai, T. Pilizota, Dynamics of Escherichia coli's passive response to a sudden decrease in external osmolarity. *Proc. Natl. Acad. Sci. U.S.A.* **113**, E5838–E5846 (2016).
71. D. S. Cayley, H. J. Guttman, M. T. Record Jr., Biophysical characterization of changes in amounts and activity of Escherichia coli cell and compartment water and turgor pressure in response to osmotic stress. *Biophys. J.* **78**, 1748–1764 (2000).
72. Y. Deng, M. Sun, J. W. Shaevitz, Direct measurement of cell wall stress stiffening and turgor pressure in live bacterial cells. *Phys. Rev. Lett.* **107**, 158101 (2011).
73. E. Bremer, R. Krämer, Responses of microorganisms to osmotic stress. *Annu. Rev. Microbiol.* **73**, 313–334 (2019).
74. U. Zarzecka, A. Zadernowska, W. Chajęcka-Wierzchowska, Effects of osmotic and high pressure stress on expression of virulence factors among Enterococcus spp. isolated from food of animal origin. *Food. Microbiol.* **102**, 103900 (2022).
75. E. Rojas, J. A. Theriot, K. C. Huang, Response of Escherichia coli growth rate to osmotic shock. *Proc. Natl. Acad. Sci. U.S.A.* **111**, 7807–7812 (2014).
76. H. N. W. Lekkerkerker, R. Tuinier, M. Vis. *Colloids and the Depletion Interaction* (Springer, 2011).
77. S. Asakura, F. Oosawa, On interaction between two bodies immersed in a solution of macromolecules. *J. Chem. Phys.* **22**, 1255–1256 (1954).
78. M. Rubinstein, *Polymer Physics* (Oxford Univ. Press, 2003).
79. S. V. Savenko, M. Dijkstra, Phase behavior of a suspension of colloidal hard rods and nonadsorbing polymer. *J. Chem. Phys.* **124**, 234902 (2006).
80. J. Schwarz-Linek, A. Winkler, L. G. Wilson, N. T. Pham, T. Schilling, W. C. K. Poon, Polymer-induced phase separation in *Escherichia coli* suspensions. *Soft Matter* **6**, 4540 (2010).
81. H. A. Kramers, Brownian motion in a field of force and the diffusion model of chemical reactions. *Physica* **7**, 284–304 (1940).
82. P. Ghosh, J. Mondal, E. Ben-Jacob, H. Levine, Mechanically-driven phase separation in a growing bacterial colony. *Proc. Natl. Acad. Sci. U.S.A.* **112**, E2166–E2173 (2015).
83. B. Sung, H. H. Wensink, E. Grelet, Depletion-driven morphological transitions in hexagonal crystallites of virus rods. *Soft Matter* **15**, 9520–9527 (2019).
84. T. Shimaya, K. A. Takeuchi, Smectic-like bundle formation of planktonic bacteria upon nutrient starvation. arXiv:2407.05031 [physics.bio-ph] (2024).
85. K. Moor, M. Diard, M. E. Sellin, B. Felmy, S. Y. Wotzka, A. Toska, E. Bakkeren, M. Arnoldini, F. Bansept, A. D. Co, T. Völler, A. Minola, B. Fernandez-Rodriguez, G. Agatic, S. Barbieri, L. Piccoli, C. Casiraghi, D. Corti, A. Lanzavecchia, R. R. Regoes, C. Loverdo, R. Stocker, D. R. Brumley, W. D. Hardt, E. Slack, High-avidity IgA protects the intestine by enchaining growing bacteria. *Nature* **544**, 498–502 (2017).
86. R. Mishra, M. Hannebelle, V. P. Patil, A. Dubois, C. Garcia-Mouton, G. M. Kirsch, M. Jan, K. Sharma, N. Guex, J. Sordet-Dessimoz, J. Perez-Gil, M. Prakash, G. W. Knott, N. Dhar, J. D. McKinney, V. V. Thacker, Mechanopathology of biofilm-like Mycobacterium tuberculosis cords. *Cell* **186**, 5135–5150.e28 (2023).
87. S. Azimi, J. Thomas, S. E. Cleland, J. E. Curtis, J. B. Goldberg, S. P. Diggle, O-specific antigen-dependent surface hydrophobicity mediates aggregate assembly type in Pseudomonas aeruginosa. *mBio* **12**, 10–1128 (2021).
88. D. Puri, X. Fang, K. R. Allison, Evidence of a possible multicellular life cycle in Escherichia coli. *iScience* **26**, 105795 (2023).
89. F. Cohn, *Untersuchungen Über Bacterien: I* (JU Kern, 1875).
90. C. Aguilar, H. Vlamakis, R. Losick, R. Kolter, Thinking about Bacillus subtilis as a multicellular organism. *Curr. Opin. Microbiol.* **10**, 638–643 (2007).
91. Y. I. Yaman, E. Demir, R. Vetter, A. Kocabas, Emergence of active nematics in chaining bacterial biofilms. *Nat. Commun.* **10**, 2285 (2019).
92. J. Schwarz-Linek, C. Valeriani, A. Cacciuto, M. E. Cates, D. Marenduzzo, A. N. Morozov, W. C. K. Poon, Phase separation and rotor self-assembly in active particle suspensions. *Proc. Natl. Acad. Sci. U.S.A.* **109**, 4052–4057 (2012).
93. M. Caldara, R. S. Friedlander, N. L. Kavanaugh, J. Aizenberg, K. R. Foster, K. Ribbeck, Mucin biopolymers prevent bacterial aggregation by retaining cells in the free-swimming state. *Curr. Biol.* **22**, 2325–2330 (2012).
94. R. M. Losick, Bacillus subtilis: A bacterium for all seasons. *Curr. Biol.* **30**, R1146–R1150 (2020).
95. M. Alhede, M. Lorenz, B. G. Fritz, P. Ø. Jensen, H. C. Ring, L. Bay, T. Bjarnsholt, Bacterial aggregate size determines phagocytosis efficiency of polymorphonuclear leukocytes. *Med. Microbiol. Immunol.* **209**, 669–680 (2020).
96. C. A. Werlang, W. G. Chen, K. Aoki, K. M. Wheeler, C. Tymm, C. J. Mileti, A. C. Burgos, K. Kim, M. Tiemeyer, K. Ribbeck, Mucin O-glycans suppress quorum-sensing pathways and genetic transformation in Streptococcus mutans. *Nat. Microbiol.* **6**, 574–583 (2021).
97. S. S. Datta, A. Preska Steinberg, R. F. Ismagilov, Polymers in the gut compress the colonic mucus hydrogel. *Proc. Natl. Acad. Sci. U.S.A.* **113**, 7041–7046 (2016).
98. A. P. Steinberg, S. S. Datta, T. Naragon, J. C. Rolando, S. R. Bogatyrev, R. F. Ismagilov, High-molecular-weight polymers from dietary fiber drive aggregation of particulates in the murine small intestine. *eLife* **8**, –e40387 (2019).
99. R. S. Eriksen, N. Mitarai, K. Sneppen, On phage adsorption to bacterial chains. *Biophys. J.* **119**, 1896–1904 (2020).
100. R. Ziege, A. M. Tsirigoni, B. Large, D. O. Serra, K. G. Blank, R. Hengge, P. Fratzl, C. M. Bidan, Adaptation of *Escherichia coli* biofilm growth, morphology, and mechanical properties to substrate water content. *ACS Biomater. Sci. Eng.* **7**, 5315–5325 (2021).
101. D. O. Serra, A. M. Richter, R. Hengge, Cellulose as an architectural element in spatially structured *Escherichia coli* biofilms. *J. Bacteriol.* **195**, 5540–5554 (2013).
102. E. Cordisco, M. I. Zanor, D. M. Moreno, D. O. Serra, Selective inhibition of the amyloid matrix of *Escherichia coli* biofilms by a bifunctional microbial metabolite. *NPJ Biofilms Microbiomes* **9**, 81 (2023).
103. D. O. Serra, A. M. Richter, G. Klauck, F. Mika, R. Hengge, Microanatomy at cellular resolution and spatial order of physiological differentiation in a bacterial biofilm. *mBio* **4**, 10-1128 (2013).
104. M. del Mar Cendra, E. Torrents, Pseudomonas aeruginosa biofilms and their partners in crime. *Biotechnol. Adv.* **49**, 107734 (2021).
105. S. S. Webster, C. K. Lee, W. C. Schmidt, G. C. L. Wong, G. A. O'Toole, Interaction between the type 4 pili machinery and a diguanylate cyclase fine-tune c-di-gmp levels during early biofilm formation. *Proc. Natl. Acad. Sci. U.S.A.* **118**, e2105566118 (2021).
106. T. L. Leighton, R. N. C. Buensuceso, P. L. Howell, L. L. Burrows, Biogenesis of *Pseudomonas aeruginosa* type iv pili and regulation of their function. *Environ. Microbiol.* **17**, 4148–4163 (2015).
107. Y. Chekli, R. J. Stevick, E. Kornobis, V. Briolat, J. M. Ghigo, C. Beloin, *Escherichia coli* aggregates mediated by native or synthetic adhesins exhibit both core and adhesin-specific transcriptional responses. *Microbiol. Spectrum* **11**, e00690-23 (2023).
108. E.-s. Q. A. Nwoko, I. N. Okeke, Bacteria autoaggregation: How and why bacteria stick together. *Biochem. Soc. Trans.* **49**, 1147–1157 (2021).

Acknowledgments: We thank T. Bhattacharjee for assistance with a preliminary version of the experiments at the inception of this project and B. Royer for assistance with imaging. We also thank T. Bhattacharjee, S. Chimileski, Z. Gitai, S. Mani, and J. M. Welch for useful discussions; H. Li, S. Mani, and Altis Biosystems for providing mucins obtained from human primary transverse colon cells; the laboratory of H. Stone for providing access to the rheometer; and the laboratories of B. Austin, B. Bassler, and Z. Gitai for providing strains of *E. coli*, *V. cholerae*, and *P. aeruginosa*, respectively. **Funding:** N.S.W. acknowledges support from NSF Center for the Physics of Biological Function grant PHY-1734030 and NIH grant R01 GM082938. S.S.D. acknowledges support from NSF grants CBET-1941716, DMR-2011750, and EF-2124863 as well as the Camille Dreyfus Teacher-Scholar and Pew Biomedical Scholars Programs, the Eric and Wendy Schmidt Transformative Technology Fund, and the Princeton Catalysis Initiative. K.R. acknowledges support from NSF grant EF-2125118. C.A.S. was supported by the Canadian Institute of Health Research (CIHR) postdoctoral fellowship (MFE-187894). **Author contributions:** S.G.L.C.: Writing—original draft, conceptualization, investigation, writing—review and editing, methodology, funding acquisition, data curation, validation, supervision, formal analysis, software, project administration, and visualization. C.A.S.: Conceptualization,

investigation, writing—review and editing, methodology, resources, and visualization. G.C.-O.: Conceptualization and investigation. K.R.: Conceptualization, writing—review and editing, methodology, resources, funding acquisition, and validation. N.S.W.: Writing—original draft, conceptualization, writing—review and editing, methodology, resources, funding acquisition, supervision, formal analysis, project administration, and visualization. S.S.D.: Writing—original draft, conceptualization, writing—review and editing, methodology, resources, funding acquisition, supervision, formal analysis, project administration, and visualization. **Competing interests:** The authors declare that they have no competing interests. **Data and materials availability:** All data needed to evaluate the conclusions in the paper are present in the paper and/or the Supplementary Materials. All movies are available at https://zenodo.org/doi/10.5281/zenodo.10966670.

Submitted 30 May 2024
Accepted 17 December 2024
Published 17 January 2025
10.1126/sciadv.adq7797

Correction (22 April 2025): Due to a production error, the figures in the original version of the article were distorted. The figures in the HTML and PDF versions of the article have been updated to resolve this issue.